RESEARCH ARTICLE

Tree Aboveground Carbon Mapping in an Indian Tropical Moist Deciduous Forest Using Object-Based Image Analysis and Very High Resolution Satellite Imagery

Neha Singh[1] · Subrata Nandy[1] · L. M. van Leeuwen[2]

Abstract

Forests' capability to sequester and store a large amount of carbon makes it imperative to assess the carbon stocked in them. The present study aimed to map the tree aboveground carbon stock of sal (*Shorea robusta*) forests of Doon valley, India using object-based image analysis (OBIA) of WorldView-2, a very high resolution satellite imagery (VHRS). The study evaluated different pan-sharpening techniques for improving the spatial resolution of WorldView-2 multispectral imagery and found that the high pass filter resolution merge technique was better compared to others. OBIA was used for image segmentation and classification. It enabled the delineation of tree crowns and canopy projection area (CPA) calculation. The overall accuracy of image segmentation and classification were found to be 72.12% and 84.82% respectively. The study unveiled that there exists a strong relationship between diameter at breast height and the CPA of trees as well as CPA and tree carbon. The average forest carbon density in the study area was found to be 108 Mg ha^{-1}. The study highlighted that OBIA of VHRS imagery coupled with field inventory can be efficiently used to quantify and map the tree carbon stock.

Keywords *Shorea robusta* · WorldView-2 · Pan-sharpening · Multi-resolution image segmentation · Canopy projection area · Carbon stock

Introduction

Forests are the most valuable natural assets on earth which functions as the planet's inherent defense against climate change. Their unparalleled ability to sequester and store vast amounts of carbon is well-documented (Gibbs et al., 2007). This stored carbon plays a crucial role in climate change mitigation. Recognizing the pivotal role of forests in mitigating climate change, precise estimation of forest carbon is essential (FAO, 2010). Challenges like inaccessibility, labor-intensive fieldwork, and time constraints underscore the need for integrating remote sensing (RS) techniques. Establishing statistical relationships between ground-based samples and satellite-derived variables is crucial for forest carbon stock mapping, following a pixel-based approach. (Dang et al., 2019; Kushwaha et al., 2014; Manna et al., 2014; Heyojoo & Nandy, 2014; Nandy et al., 2017, 2019; 2021). Nevertheless, the pixel-based approach is inadequate for assessing forest carbon stock on an individual tree level.

For estimating the carbon stock of a tree, diameter at breast height (*dbh*) is the key parameter. However, it is impossible to enumerate each tree to estimate forest carbon stock. This can be overcome by using RS-based techniques as it covers large areas. With the advent of very high resolution satellite imagery (VHRS) imagery, like IKONOS, QuickBird, Worldview-2, GeoEye, Cartosat 2S and 3, it is now possible to identify objects, like trees. The challenge arises from the limitation that optical RS satellite data cannot measure a tree *dbh* from space; they can only capture canopy reflectance values. In this context, object-based image analysis (OBIA) (Blaschke, 2010) plays a

✉ Subrata Nandy
subrato.nandy@gmail.com

Neha Singh
neha.iirs2012@gmail.com

L. M. van Leeuwen
l.m.vanleeuwen@utwente.nl

[1] Indian Institute of Remote Sensing, Indian Space Research Organisation, Department of Space, Government of India, Dehradun 248001, India

[2] Faculty of Geoinformation Science and Earth Observation (ITC), University of Twente, Enschede, The Netherlands

very significant role in the delineation of canopy projection area (CPA) of individual trees from VHRS imagery (Jing et al., 2012). Research has demonstrated a correlation between CPA and a tree *dbh* (Shimano, 1997). Consequently, establishing this relationship allows for accurate estimation of both individual tree carbon stock as well as the overall forest carbon stock. Various studies have demonstrated the potential of VHRS imagery and OBIA in conjunction with field information in mapping the tree aboveground carbon (AGC) stock effectively (Baral, 2011; Karna et al., 2015; Maharjan, 2012; Pandey et al., 2020). Baral (2011) estimated the AGC stock in a sub-tropical forest of Chitwan, Nepal using VHRS images, GeoEye and WorldView-2, and OBIA accompanied by field data. GeoEye performed better than WorldView-2 in image segmentation as well as classification in the study. Tsendbazar (2011) estimated the AGC stock of trees using VHR Geo-Eye image and OBIA, based on the allometric relationship of CPA and tree biomass, in the upper-subtropical forest of Dolakha district, Nepal. Shah and Acharya (2013) developed regression models to predict AGC stock by analyzing the relationship between CPA, derived from GeoEye imagery, and the carbon stock of trees in the Khayarkhola Watershed of Chitwan district, Central Nepal. Goncalves et al. (2019) estimated aboveground biomass (AGB) in monospecies as well as multi-species agroforestry systems of Alca-cerdo Sal and Mora, Portugal by using crown cover as an independent variable derived using contrast split segmentation and object-oriented classification of QuickBird and WorldView-2 images. Pandey et al. (2020) utilized WorldView-2 imagery and OBIA techniques to map the aboveground tree carbon stock in the Barkot forest of Uttarakhand, India. Their study demonstrated the effectiveness of this approach in accurately assessing carbon stock at the level of individual trees. Mareya et al. (2018) showcased the applicability of freely accessible high-resolution red, green, blue (RGB) satellite imagery, obtained via Google Maps, in conjunction with OBIA for accurately estimating tree canopy area and AGB in the Miombo woodlands of Harare, Zimbabwe. Workie (2017) utilized OBIA of QuickBird satellite images and in situ *dbh* measurements to estimate AGC at the individual tree level in Enschede, the Netherlands, leveraging the strong correlation between CPA and *dbh*. Hussin et al. (2014) demonstrated that VHRS imagery and OBIA-based automatic delineation and detection of tree crowns offer valuable insights into forest cover and carbon content, emphasizing the effectiveness of this method in a mixed forest in the hilly Gorkha district, Nepal, and recommending its application in diverse natural mixed and planted forests. Bagheri et al. (2021) investigated AGB and carbon stock of wild pistachio (*Pistacia atlantica*) in arid woodlands by employing OBIA of GeoEye-1, focusing on individual tree crown detection and allometric relationship development within a reserved forest area in the South Khorasan Province, East of Iran.

Maharjan (2012) integrated airborne LiDAR data and high-resolution digital camera imagery to estimate and map aboveground woody carbon stocks in the Gorkha district forests, Nepal, revealing a notable correlation of AGC with CPA and height; the accuracy of AGC stock estimation was enhanced when both variables were combined, surpassing the use of either variable alone. Mbaabu et al. (2014) estimated carbon stocks of two forest regimes, government and community-managed, in the Chitwan district of Nepal based on field data, OBIA of VHR GeoEye-1 satellite image, and airborne LiDAR data. Karna et al. (2015) combined WorldView-2 satellite imagery and airborne LiDAR data to estimate tree carbon at the species level in Nepal's Chitwan district, employing OBIA for tree canopy retrieval and supervised nearest neighbor classification methods for species-level classification. They found that WorldView-2 satellite imagery and airborne LiDAR data along with OBIA have great potential in tree species level carbon stock mapping. Wangda et al. (2019) showcased the effectiveness of integrating GeoEye and small footprint airborne LiDAR data to accurately model and estimate AGC in community forests of the Gorkha district, Nepal.

In India, Sal (*Shorea robusta*) holds significance as a vital timber species, constituting approximately 13.3% of the country's total forest area (Satya et al., 2005), and stands as a dominant tree species in both tropical moist and dry deciduous forests (Champion & Seth, 1968; Kushwaha & Nandy, 2012). In India, it occurs generally as gregarious formation in the states of Himachal Pradesh, Uttarakhand, Uttar Pradesh, Bihar, Jharkhand, Odisha, West Bengal, Assam, Tripura, Meghalaya, Madhya Pradesh and Chhattisgarh states (Champion & Seth, 1968; Roy et al., 2015; Satya et al., 2005; Troup, 1921) up to approx. 1000 m elevation and possess a significant carbon sequestration potential (Kaul et al., 2010; Navalgund et al., 2019; Pillai et al., 2019; Watham et al., 2020). Its geographical range indicates the significance of the study on carbon storage. Despite its importance, limited studies have been carried out in India's forests to quantify the carbon stock at the tree level. Hence, the current study focuses on quantifying and mapping the AGC stock in the Sal forests of the northwest Himalayan foothills of India, utilizing OBIA of VHRS imagery.

Materials and Methods

Study Area

The present study was carried out in part of the Timli forest range of Kalsi soil conservation forest division, Dehradun,

Uttarakhand, India (Subudhi & Shah, 2010). Timli forest range is further divided into blocks, viz., Aduwala, Dararit, Dharmanwala, Dhaula, Kulhal, Majari and Timli. The study area extends from 30° 19′34″–30° 25′04″ N and 77° 41′57″–77° 45′15″ E (Fig. 1), covering an area of 36 km² of Dharmanwala, Majari, Dararit and Timli blocks, in the foothills of northwest Himalaya. The area is mainly comprised of tropical moist deciduous forests (Champion & Seth, 1968), with sal as the dominated top storey species often forming pure stands. The major associated tree species of sal are *Mallotus philippensis*, *Terminalia tomentosa*, *T. bellirica* and *Lagerstroemia parviflora* (Yadav & Nandy, 2015). The terrain is relatively flat to undulating with elevation ranging from 440 to 790 m asl. The climate of the study area is tropical to sub-tropical. The temperature ranges from 2 to 40 °C with an average annual rainfall of 2000 mm. The area has a moist deciduous plant functional type (Srinet

et al., 2020) and has the potential to sequester a huge amount of carbon (Srinet et al., 2022).

Data

This study utilized WorldView-2 (WV-2) satellite imagery, consisting of a panchromatic image (PI) with a spatial resolution of 0.5 m and eight multi-spectral (MSS) bands with a spatial resolution of 2 m. The spectral bands included coastal (400–450 nm), blue (450–510 nm), green (510–580 nm), yellow (585–625 nm), red (630–690 nm), red-edge (705–745 nm), near-infrared1 (NIR1) (770–895 nm), and NIR2 (860–1040 nm), covering the electromagnetic spectrum from 400 to 1040 nm. The panchromatic (Pan) band encompassed 450 nm to 800 nm. Acquired from DigitalGlobe, Inc. on 23 October 2011, the WV-2 image was already geometrically corrected and orthorectified, featuring

Fig. 1 Location of the study area in India
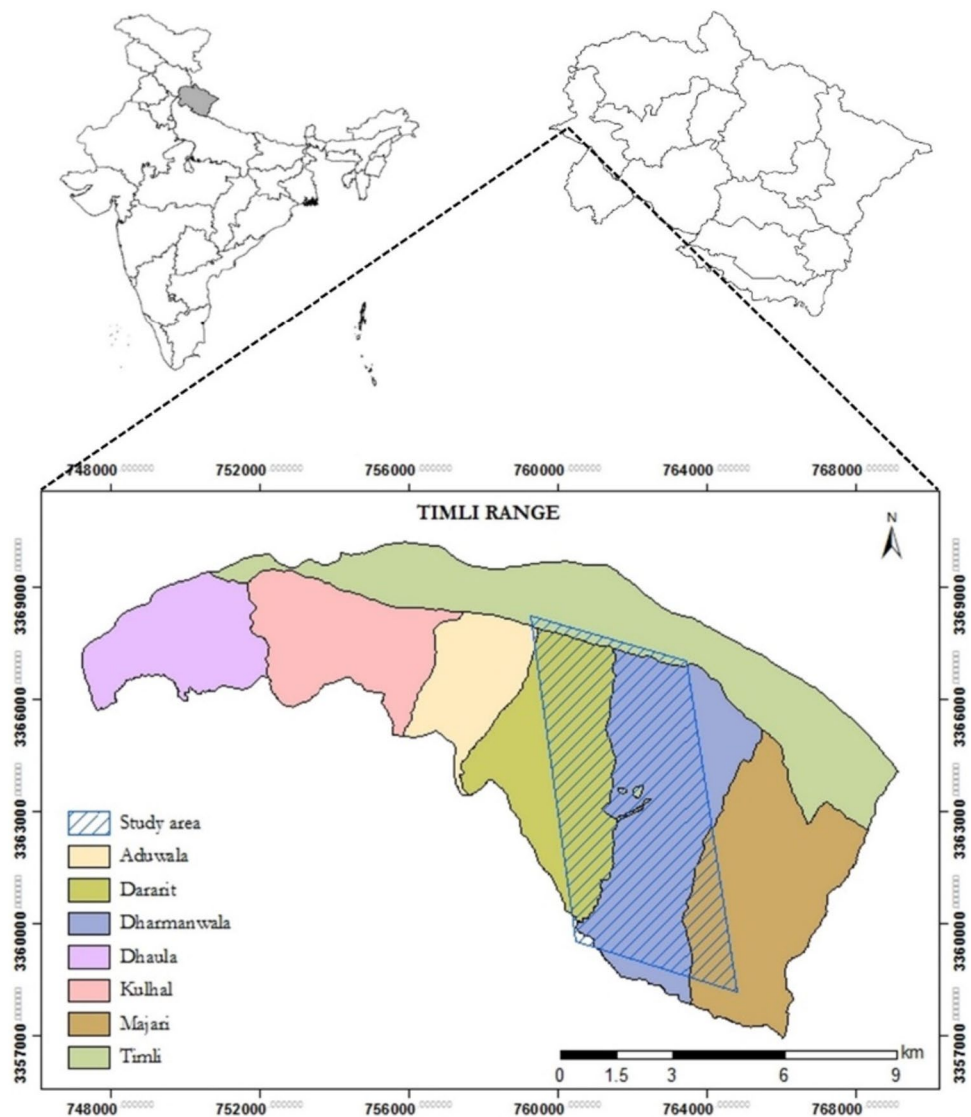
Universal Transverse Mercator (UTM) Zone 43 projection and WGS 84 datum.

Methodology

In order to get a precise estimation of carbon at the tree level, pan-sharpening was performed to enhance the spatial properties of the MSS bands of WV-2 imagery. Pan-sharpening was followed by image segmentation which was aimed at delineating the individual tree crowns to calculate CPA and estimate carbon at individual tree level. Object-based image classification was done to extract the forest class from the segmented image. Both image segmentation and classification were evaluated for their accuracies. After deriving the relationship between CPA and carbon, from the field data, the equation was used to estimate carbon at individual tree level. The regression model was also evaluated for the R^2 value. The detailed methodology is depicted in Fig. 2.

Estimation of Carbon Stock

Pan-Sharpening and Its Evaluation The WV-2 platform simultaneously captures the Pan and MSS bands, with PI at a 0.5 m resolution and eight MSS bands at a 2.0 m resolution. Seven distinct techniques, including high pass filter

(HPF) resolution merge, modified intensity hue saturation (MIHS), Ehler's fusion, wavelet resolution merge, hyperspherical colour space (HCS), principal component (PC), and Brovey transform, were employed in this study for pan-sharpening the image.

The HPF resolution merge technique, introduced by Schowengerdt (1980), extracts edge information from the high-resolution PAN band and extends it to the MSS bands. The MIHS method, as described by Nikolakopoulos (2008), approximates spectral characteristics from MSS bands while retaining spatial features from the PAN band. Utilizing an optimum index factor (OIF) (Chavez et al., 1982), only three spectral bands out of eight were included in this study. Ehler fusion method, also known as fast fourier transform (FFT) enhanced intensity, hue, saturation transform (Yuhendra et al., 2012), preserves spectral information from the MSS bands. The wavelet resolution merge technique proceeds in three steps: decomposing the high-resolution PAN band into low-resolution PIs with wavelet coefficients, replacing low-resolution PAN components with MSS bands, and then reverting the transformed PAN to its original resolution (Balcik & Sertel, 2007). HCS transformation defines colour and intensity using variables, allowing intensity adjustments without altering colours in the pan-sharpening process (Padwick et al., 2010). PC analysis transforms correlated
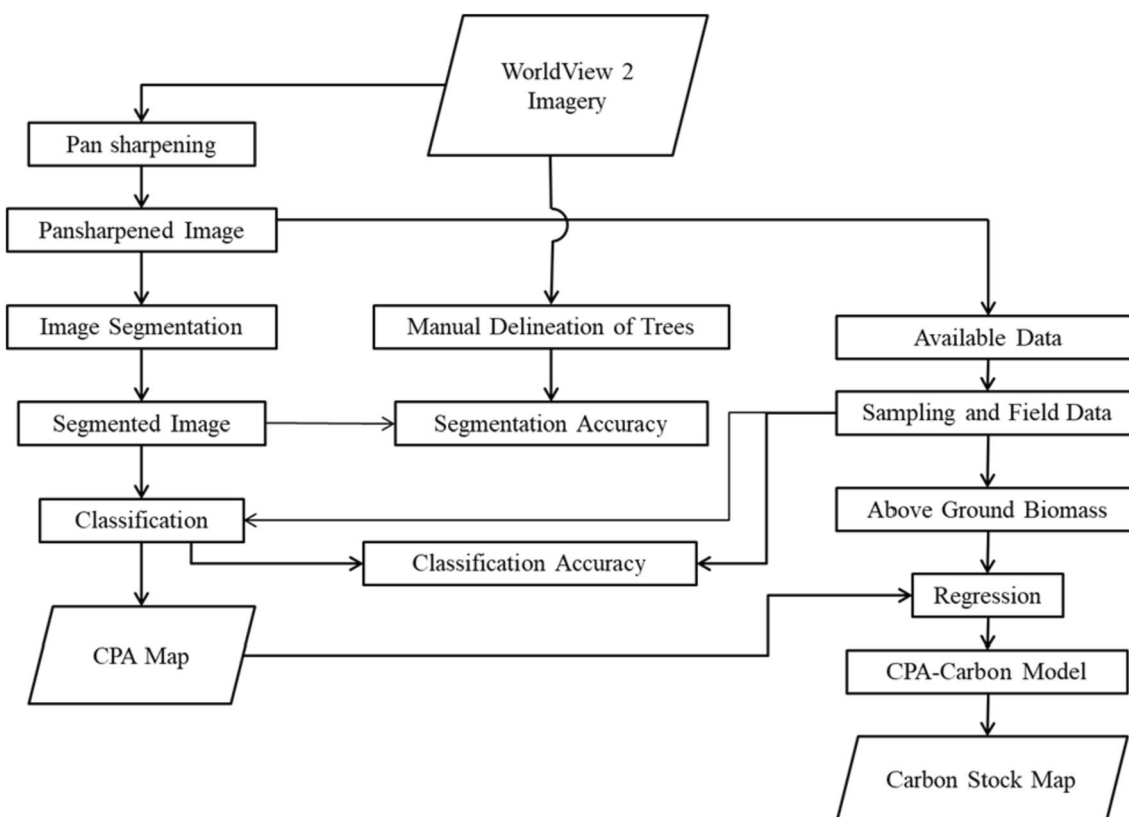

Fig. 2 Methodology followed for tree carbon estimation

bands into uncorrelated components, where high and low-resolution images are arranged into vectors, subtracting their means, and computing normalized components from resulting eigenvectors (Chavez et al., 1991). Brovey transformation involves multiplying each MSS band with the high-resolution PAN band and dividing the products by the sum of the MSS bands (Nikolakopoulos, 2008).

All these pan-sharpening techniques underwent evaluation through seven assessment methods to gauge the quality of the resultant images. The evaluation methods (Table 1) encompassed various aspects of image quality. Among the seven assessment methods, mean square error (MSE) and root mean square error (RMSE) gauged spectral distortion, while the spectral correlation coefficient provided insights into fused image spectral quality. Universal image quality index (UIQI) and relative dimensionless global error in synthesis (ERGAS) offered a comprehensive assessment of overall quality, considering both spectral and spatial aspects. Peak signal-to-noise ratio (PSNR) addressed radiometric distortion, and the spatial correlation coefficient was computed to evaluate spatial quality.

Image Segmentation Crown delineation was performed through image segmentation, a process of spatial clustering that divides the image into non-overlapping subdivisions known as segments, as described by Möller et al. (2007). Multiresolution segmentation in eCognition was used for image segmentation. Before segmentation, Gaussian filter over the image was applied. Scale parameter of 19–21 was

used to delineate the crowns from the image. After segmentation, watershed transformation of scale 7 was applied to avoid errors due to crown intermingling. Morphology was applied for edge smoothening and objects below 20 pixels were removed.

To assess the "goodness of fit" of segmentation, the D-value (Clinton et al., 2008) was computed to measure the "closeness" between pre-defined polygons (manually delineated reference polygons) and extracted polygons (segments). This metric evaluated both over-segmentation and under-segmentation. D-value ranges from 0 to 1; a D-value of zero indicates a perfect segmentation.

Over-segmentation and under-segmentation were calculated as follows:

$$\text{Over} - \text{segmentation}_{ij} = 1 - \frac{\text{Area}(x_i \cap y_i)}{\text{Area}(x_i)} \qquad (1)$$

$$\text{Under} - \text{segmentation}_{ij} = 1 - \frac{\text{Area}(x_i \cap y_i)}{\text{Area}(y_i)} \qquad (2)$$

where x_i is the reference polygon and y_j is the corresponding segment.

The D-value was calculated as:

$$D = \sqrt{\frac{\text{Over} - \text{segmentation}^2 + \text{Under} - \text{segmentation}^2}{2}} \qquad (3)$$

Table 1 Evaluation methods for pan sharpening techniques

S. no.	Method	Equation	Description
1	Mean square error	$MSE = \frac{1}{MN}\sum_{i=1}^{M}\sum_{j=1}^{N}(I_F(i,j) - I_R(i,j))^2$	MSE and RMSE are the measure of spectral distortion in the image
2	Root mean square error	$RMSE = \sqrt{MSE}$	$I_F(i,j)$ Represents the pixels of PI and $I_R(i,j)$ the pixels of fused image. M × N is the size of the image
3	Peak signal to signal noise ratio	$PSNR = 10log_{10}\left(\frac{L^2}{MSE}\right)$	PSNR is the measure of radiometric distortion in the resulting image L is the radiometric resolution of the sensor
4	Spatial correlation coefficient	$CC_{spatial}$ (P(k),M(k))	Correlation coefficient is the measure of correlation or similarity between the two images. Pearson correlation coefficient was calculated between the original MSS and fused images for assessing spectral correlation
5	Spectral correlation coefficient	$CC_{spectral}$ (P(k), M(k))	For calculating spatial correlation reference image, i.e., PI was first filtered with Laplacian filter
6	Universal image quality index	$UIQI = \left(\frac{\sigma_{xy}}{\sigma_x\sigma_y}\right)\left(\frac{2\mu_x\mu_y}{\mu_x^2+\mu_y^2}\right)\left(\frac{2\sigma_x\sigma_y}{\sigma_x^2+\sigma_y^2}\right)$	UIQI assesses the overall similarity between the reference and fused image σ_{xy} is the covariance of two images, σ_x and σ_y are the standard deviations of the images. μ_x and μ_y are the mean of the images
7	Relative dimensionless global error in synthesis	$ERGAS = 100\frac{h}{l}\sqrt{\frac{1}{N}\sum_{N=1}^{N}\left(\frac{RMSE(n)}{\mu(n)}\right)^2}$	ERGAS assesses the global quality and measures the trade-off between spectral and spatial quality, respectively h and l are the spatial resolutions of the high resolution and low resolution images, respectively. N is the number of bands and μ (n) is the mean of nth band

In this study, validation of the segmentation was done by the method suggested by Zhan et al. (2005) which assessed the overall quality, correctness, and completeness of segmentation by one-to-one matching of reference polygons and segments.

Object-Based Image Classification In this study, object-based image classification was conducted through ecognition software. The classification algorithms evaluated image objects based on defined criteria, assigning them to the most suitable class. Samples from all classes were collected through field surveys and visual interpretation. The classification accuracy was assessed using a confusion matrix, which calculated the producer's accuracy, user's accuracy, and overall accuracy, following the methodology outlined by Congalton (1991).

Carbon Stock Calculation The field inventory data was collected using a stratified random sampling approach. Forest canopy density was considered as a stratum for sampling since there was no variation in forest type. Three canopy density classes, viz., 10–40%, 40–70%, and > 70% were prepared based on the tonal differences using on-screen visual interpretation. A total of 19 plots were laid. CPA and *dbh* of trees were recorded in these sample plots.

One of the most prevalent techniques for estimating biomass is the utilization of allometric equations. For the study area, species as well as site-specific volumetric equation was used instead, due to the unavailability of an allometric equation for the area. The volumetric equation used was:

$$V = 0.03085 - 0.77794D + 8.42051D^2 + 5.91067D^3 \quad (4)$$

where V = Volume and D = Diameter at breast height.

This equation was developed by FSI (1996) to calculate the tree volume of *Shorea robusta* for the Dehradun forest division, India. Utilizing this volumetric equation, tree volumes were computed. These volumes were then multiplied by the specific gravity (FRI, 2002) and biomass expansion factor (Haripriya, 2000) to determine tree biomass. This biomass value was subsequently converted to estimate carbon, applying a conversion factor of 0.47 as recommended by IPCC (2006).

Regression Analysis and Validation In this study, a regression analysis was conducted to examine the relationship between CPA and tree carbon, with CPA serving as the independent variable and carbon as the dependent variable. A non-linear regression model was constructed using field-collected data to represent the relationship between CPA and carbon. To validate the model, a linear regression was performed between the predicted carbon values and the actual amounts calculated from the field data, using a separate test dataset collected from the field.

Results and Discussion

Pan-Sharpening

The pan-sharpening techniques were assessed both statistically and through visual interpretation of the results. Table 2 provides a summary of the statistical evaluation of the twelve applied techniques. According to the statistical analysis, the HPF resolution merge demonstrated the most favourable outcome, with HCS pan-sharpening following closely behind (Table 2). Figure 3 displays the pan-sharpened images produced by the different pan-sharpening methods.

The MSE and RMSE values indicated that the HPF resolution merge (without edge enhancement) gave the least spectral distortion. While the spectral correlation coefficient values of MIHS was least followed by Ehler's fusion.

Table 2 Results of pan sharpening evaluation

| Pan-sharpening methods	MSE	RMSE	PSNR	$CC_{spatial}$	$CC_{spectral}$	UIQI	ERGAS
HPF resolution merge (with edge enhancement)	104.56	9.99	46.43	0.93	0.71	0.64	1.15
HPF resolution merge (without edge enhancement)	103.78	9.96	46.46	0.97	0.73	0.71	1.15
Modified I H S (7,5,4)	148.8	12.10	44.64	-0.19	0.94	0.59	1.62
Ehler's fusion (NN)	114.63	10.54	45.91	0.72	0.84	0.59	1.31
Ehler's fusion (CC)	111.82	10.40	46.03	0.85	0.79	0.59	1.31
Wavelet resolution merge	109.70	10.27	46.17	0.56	0.76	0.64	1.17
HCS (with edge enhancement) (NN)	111.72	10.33	46.14	0.89	0.63	0.74	1.14
HCS (with edge enhancement) (CC)	110.51	10.26	46.22	0.96	0.66	0.75	1.14
HCS (without edge enhancement) (NN)	109.04	10.19	46.27	0.86	0.71	0.75	1.14
HCS (without edge enhancement) (CC)	106.02	10.04	46.31	0.95	0.75	0.77	1.13
Principal component	135.54	11.56	45.03	0.57	0.74	0.54	2.01
Brovey transform	266.60	16.32	41.97	0.77	0.78	0.07	13.37
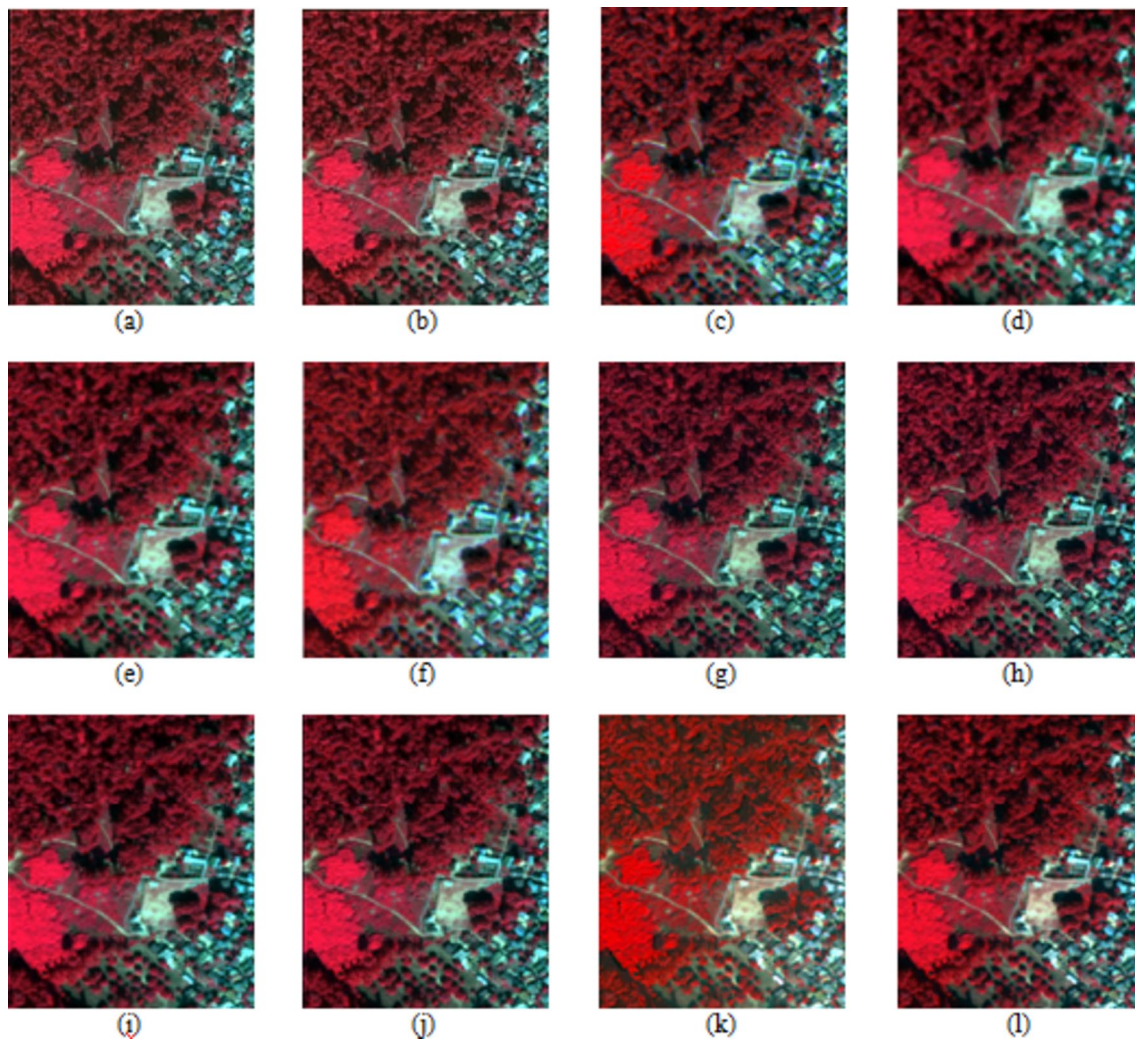
Fig. 3 Results of pan-sharpening. **a** HPF (with edge enhancement), **b** HPF (without edge enhancement), **c** MIHS, **d** Ehler fusion (NN), **e** Ehler fusion (CC), **f** Wavelet-PCA, **g** HCS (with edge enhancement –NN), **h** HCS (with edge enhancement –CC), **i** HCS (without edge enhancement –NN), **j** HCS (without edge enhancement –CC), **k** principal component, **l** Brovey transform. CC represents the cubic convolution interpolation method while NN is nearest neighbor

This signifies the efficiency of MIHS and Ehler's fusion to preserve the spectral information of the MSS bands as it approximates the spectral information. Similar studies done by Yuhendra et al. (2012) and Ghosh and Joshi (2013) on WV-2 pan-sharpening, got the least RMSE in Ehler's fusion and the highest spectral correlation in MIHS.

Among the techniques applied, HPF resolution merge (without edge enhancement) gave the highest spatial correlation with the original PI as HPF resolution merge extrapolates the edge information. Ghosh and Joshi (2013) concluded similar results where HPF gave a correlation coefficient of 0.97. In the present study, HCS and HPF gave comparable PSNR values of 46.46 and 46.31 respectively. The higher the PSNR value better the fusion result. Yuhendra et al. (2012) found Ehler's fusion to be the best while Ghosh and Joshi (2013) found that HCS gave better results

than HPF. The different pan-sharpening techniques may give different kinds of results, even if the datasets are the same (Ghosh & Joshi, 2013; Yuhendra et al., 2012). Hence, it can be concluded that the quality of pan-sharpened images might depend on the nature of the earth's surface. In the present study, HPF gave the best result compared to other methods adopted in this study.

Image Segmentation

The HPF resolution merge image from WV-2, which exhibited the best results, was used for image segmentation. Multi-resolution segmentation was performed to group pixels into homogeneous areas forming distinct objects or segments (Fig. 4). The D-value for a scale factor of 20 was 0.32, and for scale factors 19 and 21, it was 0.41 and 0.34
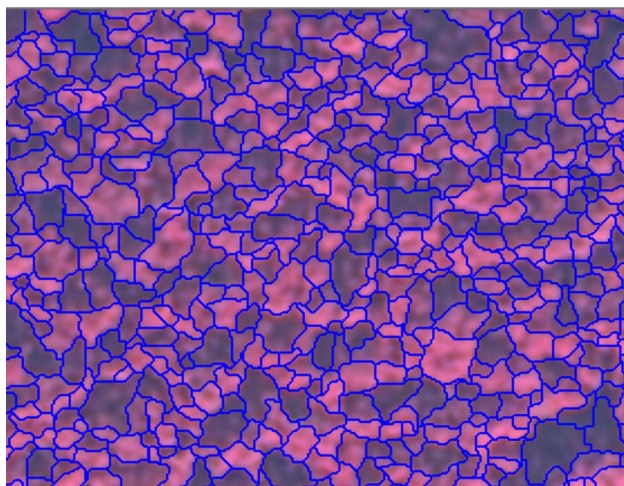
Fig. 4 Multi-resolution image segmentation

respectively. These values were comparable to the results obtained in similar studies conducted by Karna et al. (2015) and Baral (2011) in Nepalese forests, where D-values of 0.33 (Karna et al., 2015) and 0.47 (Baral, 2011) were reported. To assess segmentation accuracy, a comparison was made between manually delineated reference polygons and segmented polygons on a one-to-one basis. Out of 115 reference polygons, 83 extracted polygons matched exactly (Fig. 5). Consequently, the study achieved a segmentation accuracy of 72.17%.

Object-Based Image Classification

The objects obtained through multi-resolution segmentation were categorized based on the spectral properties of the pan-sharpened HPF resolution merge image. The classification parameters utilized included the normalized difference

vegetation index (NDVI) and the mean of NIR1. These objects were classified into four distinct categories: trees, Lantana, non-forest areas, and shadows. Given the gregarious growth of sal in the area and the dominance of sal in the top canopy, the classification was performed at a broader level and species-specific identification was not carried out. The classification results for a portion of the study area are illustrated in Fig. 6. To assess classification accuracy, samples were collected for all defined classes. An impressive overall accuracy of 84.82% was achieved. This high accuracy can be attributed to the distinct separability of the four classes from each other.

Regression Model and Validation

A non-linear regression model was developed to examine the correlation between CPA and carbon content in sal. Non-linear regression was chosen over a simple linear model based on the R^2 values. The regression analysis was conducted using 37 field observations, resulting in a correlation coefficient of 0.78 for the CPA-carbon relationship. The graphical representation of the non-linear regression between CPA and carbon is depicted in Fig. 7. The regression equation derived from the model for the relationship between CPA and carbon content in sal is as follows:

$$\text{Carbon stock} = 0.0328(\text{CPA})^2 + 0.5507(\text{CPA}) + 251.28 \tag{5}$$

The model was validated using 21 observations, where predicted carbon values were compared to calculated carbon values. The R^2 value for the model was found to be 0.87, indicating that the predicted carbon values accounted for 87% of the variation observed in the calculated carbon values obtained from field measurements.
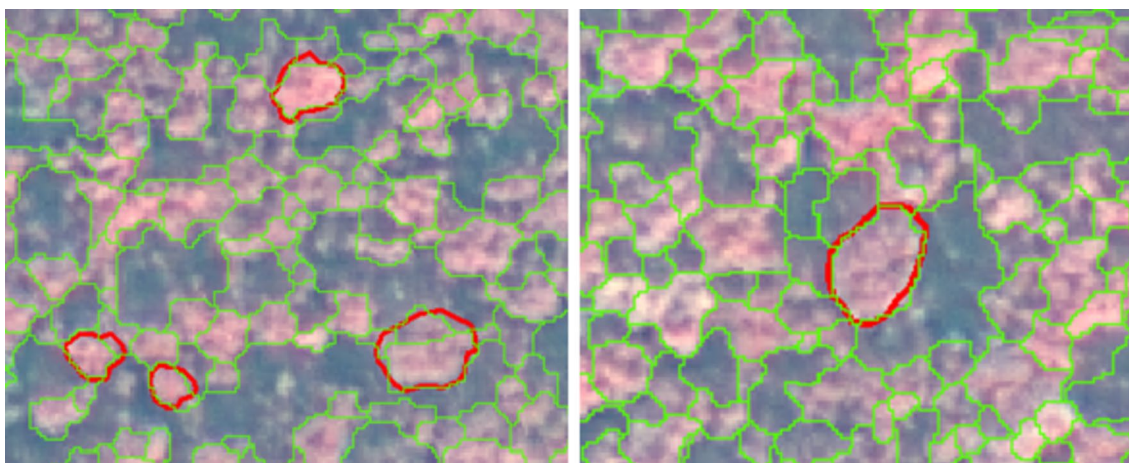

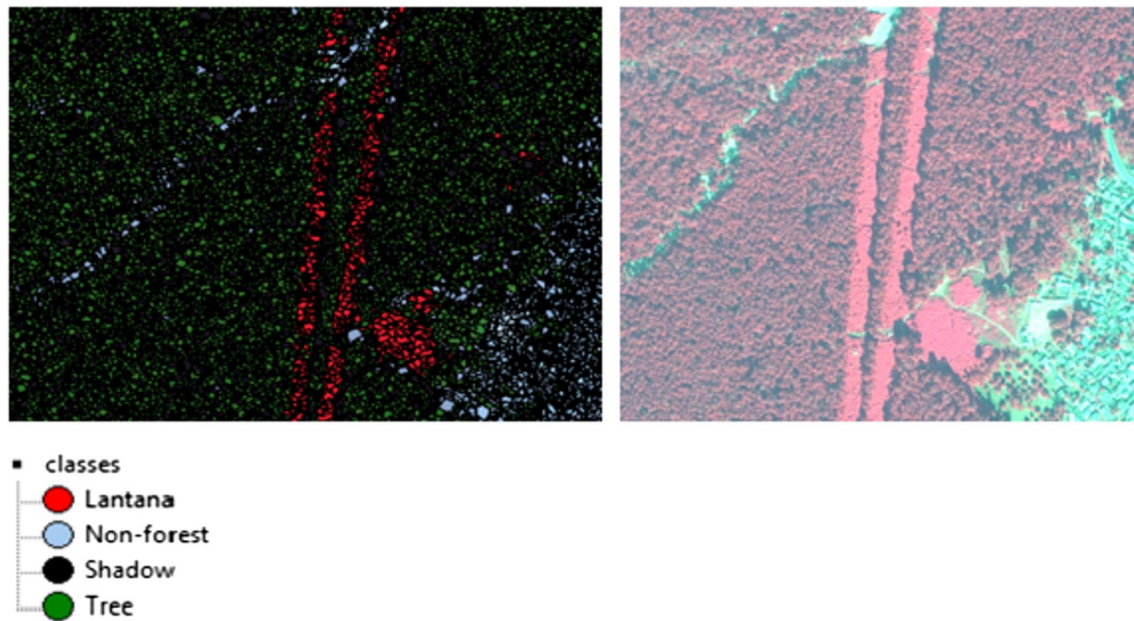**Fig. 5** Reference polygons (red) versus automatic segmentation (green) (color figure online)

- classes
  - 🔴 Lantana
  - 🔵 Non-forest
  - ⚫ Shadow
  - 🟢 Tree

Fig. 6 VHRS image and its object-based image classification

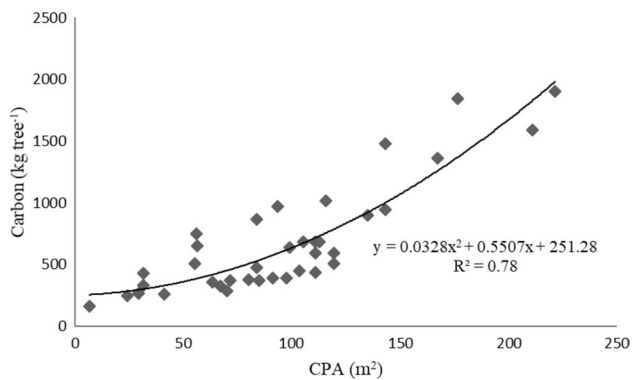$$y = 0.0328x^2 + 0.5507x + 251.28$$
$$R^2 = 0.78$$

Fig. 7 Regression between crown projection area (CPA) and carbon

Carbon Stock Mapping

The validated non-linear regression model was applied to estimate the carbon content within the study area. The study area contained an estimated 108 MgC ha^{-1}, resulting in a total estimated carbon stock of 3.81 Tg for the entire area. The distribution of carbon stock within the area is illustrated in Fig. 8, revealing that the majority of trees had less than 500 kg of carbon per tree, with only a few trees surpassing 2000 kg in carbon content.

Conclusions

This study emphasized the effectiveness of VHRS imagery in quantifying and mapping individual tree carbon stocks. The RS-based approach for assessing tree carbon stocks offers significant advantages over traditional methods. It not only provides spatial information but also enables the assessment and monitoring of carbon stocks at the individual tree level. The rise in the availability of VHRS imagery, such as WV-2, has led to the development of improved techniques like OBIA for extracting features such as CPA. The research findings underscored a substantial relationship between CPA and the carbon stock of sal trees in the northwest Himalayan foothills of India. Moreover, the study shed light on the carbon stored by individual trees of one of India's significant tree species. Hence, the integration of VHRS imagery with OBIA proves indispensable for the accurate assessment and monitoring of tree carbon stocks.

Large-scale forest carbon maps play a pivotal role in initiatives like Reducing Emissions from Deforestation and Forest Degradation (REDD+). Forest managers can enhance their carbon credits through the meticulous monitoring of forest carbon stocks. However, the study has certain limitations. Accurate delineation of CPA is crucial for estimating the carbon stock of individual trees using OBIA. In densely packed canopies, accurate segmentation of CPA becomes challenging, affecting both the classification accuracy and carbon stock assessment. Additionally, this approach allows mapping only the carbon stock of top canopy tree species. Co-dominant or suppressed trees
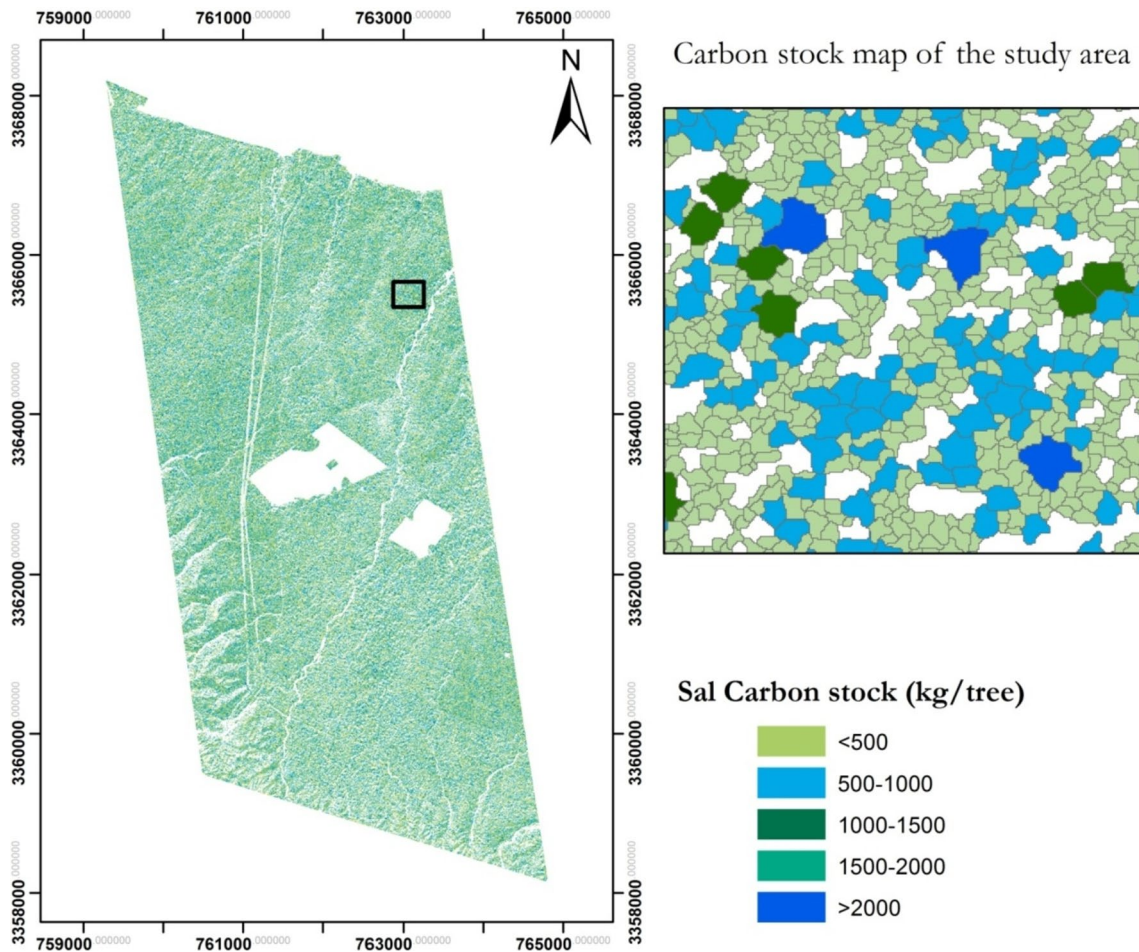
Fig. 8 Carbon stock at individual tree level

remain invisible in the imagery and, therefore, cannot be mapped. Developing local allometric equations is essential for improving the assessment of field biomass and carbon. Furthermore, the integration of airborne LiDAR data could have provided a more precise estimation of carbon stock by incorporating height information alongside VHRS imagery.

Declarations

Conflict of interest The authors declare no conflict of interest.

References

Subudhi, S.P., & Shah, R. (2010). *Working plan of Kalsi soil conservation forest division*, Kalsi Shivalik Circle (2009–10 to 2018–19). Government of Uttarakhand, Dehradun.

Bagheri, R., Shataee, S., & Erfanifard, S. Y. (2021). Canopy based aboveground biomass and carbon stock estimation of wild pistachio trees in arid woodlands using Geoeye-1 images. *Journal of Agricultural Science and Technology, 23*(1), 107–123.

Balcik, F. B., & Sertel, E. (2007). Wavelet-based image fusion of Landsat ETM images: A case study for different landscape categories of İstanbul. In *ISPRS commission VII, WG2 & WG7, conference on information extraction from SAR and optical data, with emphasis on developing countries*, 16–18 May 2007 Istanbul, Turkey.

Baral, S. (2011). Mapping carbon stock using high resolution satellite images in sub-tropical forest of Nepal. Dissertation, Faculty of Geo-Information and Earth Observation (ITC), University of Twente, Enschede, The Netherlands.

Blaschke, T. (2010). Object based image analysis for remote sensing. *ISPRS Journal of Photogrammetry and Remote Sensing, 65*(1), 2–16. https://doi.org/10.1016/j.isprsjprs.2009.06.004

Champion, H. G., & Seth, S. K. (1968). *A revised survey of the forest types of India*. Delhi: Manager of Publications.

Chavez, P. S., Jr., Berlin, G. L., & Sowers, L. B. (1982). Statistical method for selecting Landsat MSS ratios. *Journal of Applied Photographic Engineering, 8*(1), 23–30.

Chavez, P. S., Jr., Sides, S. C., & Anderson, J. A. (1991). Comparison of three different methods to merge multiresolution and multi-spectral data—Landsat TM and SPOT Panchromatic. *Photogrammetric Engineering and Remote Sensing, 57*(3), 295–303.

Clinton, N., Holt, A., Yan, L., & Gong, P. (2008). An accuracy assessment measure for object based image segmentation. *The International Archives of the Photogrammetry, Remote Sensing and Spatial Information Sciences, 37*, 1189–1194.

Congalton, R. G. (1991). A review of assessing the accuracy of classifications of remotely sensed data. *Remote Sensing of Environment, 37*(1), 35–46.

Dang, A. T. N., Nandy, S., Srinet, R., Luong, N. V., Ghosh, S., & Kumar, A. S. (2019). Forest aboveground biomass estimation using machine learning regression algorithm in Yok Don National Park, Vietnam. *Ecological Informatics, 50*, 24–32. https://doi.org/10.1016/j.ecoinf.2018.12.010

FAO. (2010). *Managing forests for climate change* (p. 20). Rome, Italy: Food and Agriculture Organization.

FRI. (2002). *Indian woods: Their identification, properties and uses*, Vol. I-VI (Revised edition). Forest Research Institute, Dehradun, Indian Council of Forestry Research and Education, Ministry of Environment and Forests, Government of India.

FSI. (1996). *Volume equations for forests of India, Nepal and Bhutan*. Forest Survey of India, Dehradun, Ministry of Environment and Forests, Government of India.

Ghosh, A., & Joshi, P. K. (2013). Assessment of pan-sharpened very high-resolution WorldView-2 images. *International Journal of Remote Sensing, 34*(23), 8336–8359. https://doi.org/10.1080/01431161.2013.838706

Gibbs, H. K., Brown, S., Niles, J. O., & Foley, J. A. (2007). Monitoring and estimating tropical forest carbon stocks: Making REDD a reality. *Environmental Research Letters, 2*(4), 045023. https://doi.org/10.1088/1748-9326/2/4/045023

Gonçalves, A. C., Sousa, A. M., & Mesquita, P. (2019). Functions for aboveground biomass estimation derived from satellite images data in Mediterranean agroforestry systems. *Agroforestry Systems, 93*, 1485–1500. https://doi.org/10.1007/s10457-018-0252-4

Haripriya, G. S. (2000). Estimates of biomass in Indian forests. *Biomass and Bioenergy, 19*(4), 245–258. https://doi.org/10.1016/S0961-9534(00)00040-4

Heyojoo, B. P., & Nandy, S. (2014). Estimation of above-ground phytomass and carbon in tree resources outside the forest (TROF): A geo-spatial approach. *Banko Janakari, 24*(1), 34–40. https://doi.org/10.3126/banko.v24i1.13488

Hussin, Y. A., Gilani, H., van Leeuwen, L., Murthy, M. S. R., Shah, R., Baral, S., Tsendbazar, N. E., Shrestha, S., Shah, S. K., & Qamer, F. M. (2014). Evaluation of object-based image analysis techniques on very high-resolution satellite image for biomass estimation in a watershed of hilly forest of Nepal. *Applied Geomatics, 6*, 59–68. https://doi.org/10.1007/s12518-014-0126-z

IPCC. (2006). *IPCC guidelines for national greenhouse gas inventories*. The Intergovernmental Panel on Climate Change, Kanagawa, Japan.

Jing, L., Hu, B., Noland, T., & Li, J. (2012). An individual tree crown delineation method based on multi-scale segmentation of imagery. *ISPRS Journal of Photogrammetry and Remote Sensing, 70*, 88–98. https://doi.org/10.1016/j.isprsjprs.2012.04.003

Karna, Y. K., Hussin, Y. A., Gilani, H., Bronsveld, M. C., Murthy, M. S. R., Qamer, F. M., Karky, B. S., Bhattarai, T., Aigong, X., & Baniya, C. B. (2015). Integration of WorldView-2 and airborne LiDAR data for tree species level carbon stock mapping in Kayar Khola watershed, Nepal. *International Journal of Applied Earth Observation and Geoinformation, 38*, 280–291. https://doi.org/10.1016/j.jag.2015.01.011

Kaul, M., Mohren, G. M. J., & Dadhwal, V. K. (2010). Carbon storage and sequestration potential of selected tree species in India. *Mitigation and Adaptation Strategies for Global Change, 15*(5), 489–510. https://doi.org/10.1007/s11027-010-9230-5

Kushwaha, S. P. S., & Nandy, S. (2012). Species diversity and community structure in sal (*Shorea robusta*) forests of two different rainfall regimes in West Bengal, India. *Biodiversity and Conservation, 21*(5), 1215–1228. https://doi.org/10.1007/s10531-012-0264-8

Kushwaha, S. P. S., Nandy, S., & Gupta, M. (2014). Growing stock and woody biomass assessment in Asola-Bhatti Wildlife Sanctuary, Delhi, India. *Environmental Monitoring and Assessment, 186*(9), 5911–5920. https://doi.org/10.1007/s10661-014-3828-0

Maharjan, S. (2012). Estimation and mapping above ground woody carbon stocks using lidar data and digital camera imagery in the hilly forests of Gorkha, Nepal. Dissertation, Faculty of Geo-Information and Earth Observation (ITC), University of Twente, Enschede, The Netherlands.

Manna, S., Nandy, S., Chanda, A., Akhand, A., Hazra, S., & Dadhwal, V. K. (2014). Estimating aboveground biomass in *Avicennia marina* plantation in Indian Sundarbans using high-resolution satellite data. *Journal of Applied Remote Sensing, 8*(1), 083638. https://doi.org/10.1117/1.JRS.8.083638

Mareya, H. T., Tagwireyi, P., Ndaimani, H., Gara, T. W., & Gwenzi, D. (2018). Estimating tree crown area and aboveground biomass in miombo woodlands from high-resolution RGB-only imagery. *IEEE Journal of Selected Topics in Applied Earth Observations and Remote Sensing, 11*(3), 868–875. https://doi.org/10.1109/JSTARS.2018.2799386

Mbaabu, P. R., Hussin, Y. A., Weir, M., & Gilani, H. (2014). Quantification of carbon stock to understand two different forest management regimes in Kayar Khola watershed, Chitwan, Nepal. *Journal of the Indian Society of Remote Sensing, 42*, 745–754. https://doi.org/10.1007/s12524-014-0379-3

Möller, M., Lymburner, L., & Volk, M. (2007). The comparison index: A tool for assessing the accuracy of image segmentation. *International Journal of Applied Earth Observation and Geoinformation, 9*(3), 311–321. https://doi.org/10.1016/j.jag.2006.10.002

Nandy, S., Ghosh, S., Kushwaha, S. P. S., & Kumar, A. S. (2019). *Remote sensing-based forest biomass assessment in northwest Himalayan landscape* (pp. 285–311). Singapore: Springer. https://doi.org/10.1007/978-981-13-2128-3_13

Nandy, S., Singh, R., Ghosh, S., Watham, T., Kushwaha, S. P. S., Kumar, A. S., & Dadhwal, V. K. (2017). Neural network-based modelling for forest biomass assessment. *Carbon Management, 8*(4), 305–317. https://doi.org/10.1080/17583004.2017.1357402

Nandy, S., Srinet, R., & Padalia, H. (2021). Mapping forest height and aboveground biomass by integrating ICESat-2, Sentinel-1 and Sentinel-2 data using random forest algorithm in northwest Himalayan foothills of India. *Geophysical Research Letters, 48*(14), e2021GL093799. https://doi.org/10.1029/2021GL093799

Navalgund, R. R., Kumar, A. S., & Nandy, S. (2019). *Remote sensing of Northwest Himalayan ecosystems*. Singapore: Springer. https://doi.org/10.1007/978-981-13-2128-3

Nikolakopoulos, K. G. (2008). Comparison of nine fusion techniques for very high resolution data. *Photogrammetric Engineering and Remote Sensing, 74*(5), 647–659. https://doi.org/10.14358/PERS.74.5.647

Padwick, C., Deskevich, M., Pacifici, F., & Smallwood, S. (2010). WorldView-2 pan-sharpening. In *ASPRS 2010 annual conference*, San Diego, California, April 26–30, 2010.

Pandey, S. K., Chand, N., Nandy, S., Muminov, A., Sharma, A., Ghosh, S., & Srinet, R. (2020). High-resolution mapping of forest carbon stock using object-based image analysis (OBIA) technique. *Journal of the Indian Society of Remote Sensing, 48*, 865–875. https://doi.org/10.1007/s12524-020-01121-8

Pillai, N. D., Nandy, S., Patel, N. R., Srinet, R., Watham, T., & Chauhan, P. (2019). Integration of eddy covariance and process-based model for the intra-annual variability of carbon fluxes in an Indian tropical forest. *Biodiversity and Conservation, 28*(8–9), 2123–2141. https://doi.org/10.1007/s10531-019-01770-3

Roy, P. S., Behera, M. D., Murthy, M. S. R., Roy, A., Singh, S., Kushwaha, S. P. S., Jha, C. S., Sudhakar, S., Joshi, P. K., Sudhakar Reddy, Ch., Gupta, S., Pujar, G., Dutt, C. B. S., Srivastava, V. K., Porwal, M. C., Tripathi, P., Singh, J. S., Chitale, V., Skidmore, A. K.,…Ramachandran, R. M. (2015). New vegetation type map of India prepared using satellite remote sensing: Comparison with global vegetation maps and utilities. *International Journal of Applied Earth Observation and Geoinformation, 39*, 142–159. https://doi.org/10.1016/j.jag.2015.03.003

Satya, Upreti, D. K., & Nayaka, S. (2005). Shorea robusta—An excellent host tree for lichen growth in India. *Current Science, 89*(4), 594–595.

Schowengerdt, R. A. (1980). Reconstruction of multispatial, multispectral image data using spatial frequency content. *Photogrammetric Engineering and Remote Sensing, 46*(10), 1325–1334.

Shah, S. K., & Acharya, H. (2013). Modelling the relationship between canopy projection area and above-ground carbon stock of intermingled canopy trees using high-resolution satellite imagery. *Banko Janakari, 23*(2), 20–29.

Shimano, K. (1997). Analysis of the relationship between DBH and crown projection area using a new model. *Journal of Forestry Research, 2*(4), 237–242. https://doi.org/10.1007/BF02348322

Srinet, R., Nandy, S., Padalia, H., Ghosh, S., Watham, T., Patel, N. R., & Chauhan, P. (2020). Mapping plant functional types in Northwest Himalayan foothills of India using random forest algorithm in Google Earth Engine. *International Journal of Remote Sensing, 41*(18), 7296–7309. https://doi.org/10.1080/01431161.2020.1766147

Srinet, R., Nandy, S., Watham, T., Padalia, H., & Patel, N. R. (2022). Coupling Earth observation and eddy covariance data in light-use efficiency based model for estimation of forest productivity. *Geocarto International, 37*(25), 7716–7732. https://doi.org/10.1080/10106049.2021.1983032

Troup, R. S. (1921). *The silviculture of Indian trees* (Vol. I). Clarendon Press.

Tsendbazar, N. E. (2011). Object based image analysis of geo-eye VHR data to model above ground carbon stock in Himalayan mid-hill forests, Nepal. Dissertation, Faculty of Geo-Information and Earth Observation (ITC), University of Twente, Enschede, The Netherlands.

Wangda, P., Hussin, Y. A., Bronsveld, M. C., & Karna, Y. K. (2019). Species stratification and upscaling of forest carbon estimates to landscape scale using GeoEye-1 image and lidar data in subtropical forests of Nepal. *International Journal of Remote Sensing, 40*(20), 7941–7965. https://doi.org/10.1080/01431161.2019.1607981

Watham, T., Srinet, R., Nandy, S., Padalia, H., Sinha, S. K., Patel, N. R., & Chauhan, P. (2020). Environmental control on carbon exchange of natural and planted forests in Western Himalayan foothills of India. *Biogeochemistry, 151*, 291–311.

Workie, T. G. (2017). Estimating forest above-ground carbon using object-based analysis of very high spatial resolution satellite images. *African Journal of Environmental Science and Technology, 11*(12), 587–600. https://doi.org/10.5897/AJEST2017.2358

Yadav, B. K. V., & Nandy, S. (2015). Mapping aboveground woody biomass using forest inventory, remote sensing and geostatistical techniques. *Environmental Monitoring and Assessment, 187*(5), 1–12. https://doi.org/10.1007/s10661-015-4551-1

Yuhendra, Alimuddin, I., Sumantyo, J. T. S., & Kuze, H. (2012). Assessment of pan-shrpening methods applied to image fusion of remotely sensed multi-data band. *International Journal of Applied Earth Observation and Geoinformation, 18*, 165–175. https://doi.org/10.1016/j.jag.2012.01.013

Zhan, Q., Molenaar, M., Tempfli, K., & Shi, W. (2005). Quality assessment for geo-spatial objects derived from remotely sensed data. *International Journal of Remote Sensing, 26*(14), 2953–2974. https://doi.org/10.1080/01431160500057764